Desalination and Water Treatment
www.deswater.com

doi: 10.1080/19443994.2013.791784

51 (2013) 7101–7108
November

Taylor & Francis
Taylor & Francis Group

Photocatalytic degradation of methylene blue by visible-light-driven yttrium-doped mesoporous titania coated magnetite photocatalyst

Shuhua Yao[a], Shuangping Song[a], Zhongliang Shi[a,*], Shaofeng Wang[b,*]

[a]*School of Applied Chemistry, Shenyang University of Chemical Technology, Shenyang 110142, China*
Tel./Fax: +86 24 8938 3296; email: shzhl2000@163.com
[b]*Institute of Applied Ecology, Chinese Academy of Sciences, Shenyang 110016, China*

Received 31 December 2011; Accepted 24 February 2013

ABSTRACT

A novel kind of visible-light-driven photocatalyst ($Y/MTiO_2/Fe_3O_4$) with yttrium-doped mesoporous titania ($Y/MTiO_2$) shell and a magnetite core was prepared by coating photoactive $Y/MTiO_2$ onto a magnetic Fe_3O_4 core through the hydrolysis of tetrabutyltitanate ($Ti(OBu)_4$) with precursors of $Y(NO_3)_3{\cdot}6H_2O$ and ($Ti(OBu)_4$) in the presence of Fe_3O_4 particles, the $MTiO_2$ shell was for photocatalysis, the Fe_3O_4 core was for separation by the magnetic field and the doped Y was used to enhance the photocatalytic activity of $MTiO_2$. The photocatalytic activities of obtained photocatalysts under visible light were estimated by measuring the degradation rate of methylene blue (50 mg/L) in an aqueous solution. The results showed that the prepared photocatalyst was activated by visible light and used as effective catalyst in photooxidation reactions. In addition, the possibility of cyclic usage of the prepared photocatalyst was also confirmed. Moreover, the photocatalyst could be easily recovered from the medium by an external magnetic field and be reused without any mass loss. It can therefore be potentially applied for the treatment of water contaminated by organic pollutants.

Keywords: Mesoporous titania; Magnetite; Yttrium-doping; Photocatalytic degradation; Methylene blue

1. Introduction

Within the ecosystem, colored wastewater released in textile effluents is a dramatic source of pollution, eutrophication, and perturbations in aquatic life. Methyl blue (MB) is the representative substance of dye compounds, its structure has the benzene ring, which presents a strong inhibitive function for biologic degradation, so they are very difficult to be degraded into small inorganic molecules by using common methods. Degradation of these toxic substances by photocatalysis in aqueous medium could be the basis of the waste treatment method [1–3].

Titania, an inexpensive, non-toxic and biocompatible material, has attracted much attention for its potential application in decomposition of various environmental pollutants in both gaseous and liquid phases [4–7]. Compared with titania, mesoporous titania, which displays better photocatalytic activity because of its high specific surface area and uniform pore diameter, has therefore received much interest in photocatalysis [8,9]. However, in field applications, there are at least two obvious problems arising from using fine mesoporous titania powders: (1) separation

*Corresponding author.

of fine particles of mesoporous TiO_2 used after the treatment process and the recycling of the photocatalyst; (2) low photoefficiency [10]. Many techniques [11,12] were proposed for the preparation of mesoporous films of TiO_2 to eliminate the first problem. In order to improve the photocatalytic activity of fine TiO_2 powders, many researches [13–18] have been carried out. These results showed that selective metal ion doping was one of the effective means, which could provide a framework to more easily incorporate the photocatalytic and solar efficiency of this material. Rare earth metals having incompletely occupied 4f and empty 5d orbitals often serve as catalyst or catalysis promoter. Some results showed that the photocatalytic activity of TiO_2 could be improved, because of the doping of some rare earth metals [19–21]. Besides, it has been proved that yttrium, as one of the rare earth metals, has the ability to enhance the photocatalytic activity of TiO_2 [22].

In the current work, a series of yttrium-doped mesoporous titania ($Y/MTiO_2$)/Fe_3O_4) composites ($Y/MTiO_2$ coatings on Fe_3O_4) were prepared by a template method using $Y(NO_3)_3{\cdot}6H_2O$ and tetrabutyltitanate ($Ti(OBu)_4$) as precursors and Pluronic P123 as template, where Fe_3O_4 was synthesized by co-precipitation of iron(II) and iron(III) in the presence of ammonium hydroxide. In this article, the photocatalytic activity of $Y/MTiO_2/Fe_3O_4$ was evaluated by photodegradation of MB over these obtained samples under visible light irradiation. The regeneration of TiO_2 photocatalyst is one of the key steps to making heterogeneous photocatalysis technology for practical applications. The separation problem of the prepared photocatalyst has been solved, after photodegradation, the magnetic composite can be separated from the medium by a simple magnetic process, so the photocatalyst can be reused easily without any mass loss. Moreover, the activity of $MTiO_2$ was not depressed by doping the magnetic photocatalyst with yttrium. It can therefore be potentially applied for the treatment of water contaminated by organic pollutants.

2. Experimental

2.1. Synthesis procedure

2.1.1. Preparation of Y-doped $MTiO_2$ nanoparticles

In a typical synthesis, 0.01 mol of $Ti(OBu)_4$ was added to a solution containing 1.0 g of Pluronic P123 ($EO_{20}PO_{70}EO_{20}$, Aldrich Chemical Co., Milwaukee, WI) and 10.0 g of anhydrous ethanol. To this solution, the appropriate amount of $Y(NO_3)_3{\cdot}6H_2O$ was added prior to the hydrolysis of $Ti(OBu)_4$ under vigorous stirring for the synthesis of Y-doped mesoporous TiO_2. The resulting sol was gelled in an open Petri dish at 50 °C in air for four days. The as-made bulk samples were then calcined at 500 °C for 2 h in air at the heating rate of 10 °C/min to remove the surfactant.

2.1.2. Preparation of $Y/MTiO_2/Fe_3O_4$ nanoparticles

$Y/MTiO_2/Fe_3O_4$ nanoparticles were prepared as follows: appropriate amount of magnetite particles synthesized by chemical co-precipitation of iron(II) and iron(III) in the presence of ammonium hydroxide were dispersed in $Y/MTiO_2$ sols in an ultrasonic bath for 2 h. Then, it was dried into powders in a rotatory evaporator under vacuum at 75 °C and calcined at 500 °C for 2 h. The composition of the prepared samples was determined to be $Y:Fe_3O_4:MTiO_2 = 0.32:25.0:74.68$–$0.73:30.0:69.27$.

2.2. Characterization

The specific surface area and pore volumes of samples were obtained by nitrogen adsorption–desorption at 77 K using the BET method with a micromeritics 2000 instrument (ASAP 2000, Micromeritics, USA). The micrograph of the prepared sample was examined with a transmission electron microscopy (TEM, JEM 2000 EX). X-ray diffraction (XRD) was used for identification of the crystalline phases of the prepared samples. The XRD patterns were recorded in the range of $2\theta = 20$–$80°$ by step scanning with a Rigaku D/max-r B X-ray diffractometer using graphite monochromatic copper radiation (Cu–Kα) at 40 kV, 30 mA. UV–vis adsorption spectroscopy measurements were performed by using a UV–vis diffuse reflectance spectrophotometer (Shimadzu UV-2550). Reflectance spectra were referenced to $BaSO_4$.

2.3. Photocatalytic degradation studies

The photocatalytic activities of the prepared catalysts under visible light irradiation were estimated by measuring the degradation rate of MB (50 mg/L) in an aqueous solution. Experiments were carried out using a magnetically stirred quartz reactor and a 150 W metal halide lamp as the light source at ambient temperature of ca. 20 °C. To limit the irradiation wavelength, the light beam was passed through a 410 nm cut filter (L41) to assure cut-off wavelengths shorter than 410 nm. One gram of photocatalyst was added under stirring into 500 mL of MB whose initial concentration was 50 mg/L. Sixty-minute adsorption time in dark condition was allowed before the start of photoreactions. Then, samples of the suspension were withdrawn after a definite time interval, and the

photocatalysts in the suspension were recovered by an external magnetic process. Then the samples were analyzed for residual MB concentration using a UV–vis spectrophotometer (UV762, Shanghai Analysis Co.) at 664 nm. To compare the photocatalytic activity of $Y/MTiO_2/Fe_3O_4$, $MTiO_2$, and $MTiO_2/Fe_3O_4$ powders were also tested. The $Y/MTiO_2/Fe_3O_4$ sample was used repeatedly, and each cycle lasted 4 h. Before the beginning of the next cycle, the remaining solution was replaced by fresh MB solution with 50 mg/L.

3. Results and discussion

3.1. TEM studies

A TEM micrograph of $Y/MTiO_2/Fe_3O_4$ was shown in Fig. 1. It could be seen from the micrograph that the coating of $Y/MTiO_2$ on the surface of the magnetite particles resulted in the formation of a core–shell type structure, in which most Fe_3O_4 particles as the core and the $Y/MTiO_2$ as the shell, and the size of the particles was around 40 nm.

3.2. XRD analysis

To obtain information on the crystal structure of the $Y/MTiO_2/Fe_3O_4$ photocatalysts, XRD patterns were measured. The XRD patterns of prepared samples were shown in Fig. 2. Fig. 2(a) shows XRD pattern of the Fe_3O_4, presenting the characteristic peaks of cubic spinel structure. It could also be seen from Fig. 2 that all samples prepared have the anatase structure, with no significant rutile component. The diffraction peaks at 25.28°, 37.80°, 48.05°, and 55.07° are consistent with the (1 0 1), (0 0 4), (2 0 0), and (1 0 5) peaks of anatase titania. Fig. 2(c) and (d) shows that the Fe_3O_4 maintained cubic spinel structure. This illuminated that the magnetic properties of Fe_3O_4 were basically invariable. The XRD results suggested that the Y-doping has little influence on the nature of crystal formation. No characteristic peak of Y oxide was found in the XRD patterns implying either Y ions were incorporated in the crystallinity of $MTiO_2$, or Y oxide was very small and highly dispersed.

3.3. Nitrogen adsorption–desorption analysis

Information about specific surface area, pore volume, and BET surface area of catalysts were summarized in Table 1. As shown in Table 1, the deposited iron oxide contributed to a decrease in the N_2-BET surface area, mesoporous volume, and microporous volume. As Fe_3O_4 has a relatively small surface area and microporous volume (62.2 m^2/g and 0.012 cm^3/g, respectively), its presence in the composites should cause a decrease in the surface area and microporous volume compared to pure $MTiO_2$ and $Y/MTiO_2/Fe_3O_4$ photocatalyst. The N_2 adsorption–desorption isotherms and Barret–Joyner–Halenda (BJH) pore size distribution plots (calculated from the adsorption branch) of pure mesoporous TiO_2 and $Y/MTiO_2/Fe_3O_4$ were shown in Fig. 3. The adsorption–desorption isotherms of all samples are of type IV with H2 hysteresis loop with stepwise adsorption and desorption [23]. The sharp decline in the desorption curve and the hysteresis loop at high relative pressure are indicative of mesoporosity. During the process of

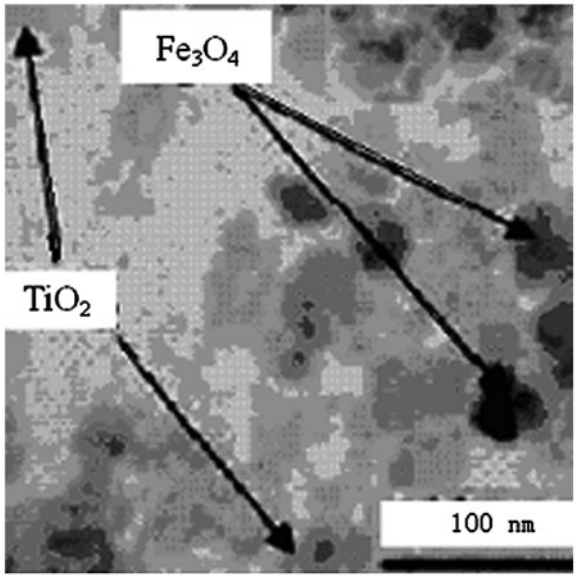

Fig. 1. TEM micrograph of 0.20 mol% $Y/MTiO_2/Fe_3O_4$.

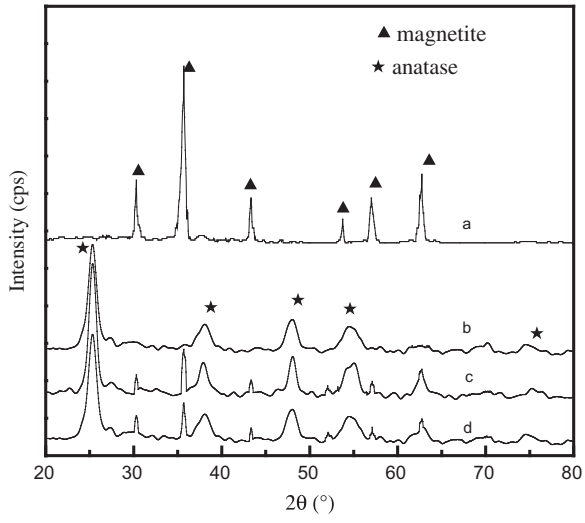

Fig. 2. XRD patterns of samples (a) Fe_3O_4, (b) $MTiO_2$, (c) $MTiO_2/Fe_3O_4$, and (d) 0.20 mol% $Y/MTiO_2/Fe_3O_4$.

Table 1
Microstructure of pure Fe_3O_4, $MTiO_2$ and 0.20 mol% Y/$MTiO_2$/Fe_3O_4 photocatalysts

Sample	S_{BET} (m^2/g)	Mesoporous volume (cm^3/g)	Microporous volume (cm^3/g)
Fe_3O_4	62.2	0.365	0.012
$MTiO_2$	161.5	0.846	0.058
Y/$MTiO_2$/Fe_3O_4	143.3	0.712	0.055

adsorption, single-molecular layer adsorption occurred at relatively low pressure and then multi-molecular layer adsorption occurred at higher pressure. The larger the sample pore sizes, the higher the pressure of capillary cohesion that occurred [24]. As shown in Fig. 3, the capillary cohesion of mesoporous TiO_2 occurred at the higher pressure and that of Y/$MTiO_2$/Fe_3O_4 occurred at the lower pressure. It suggested that the sample mesoporous TiO_2 had the larger pore size and Y/$MTiO_2$/Fe_3O_4 had the smaller pore size. The narrow pore size distribution curves indicated that the present materials have uniform pore channels.

3.4. UV–vis diffuse reflectance spectra analysis

UV–vis diffuse reflectance spectra were used to characterize the light absorption ability of the prepared photocatalysts. Fig. 4 shows the diffuse reflectance spectra for different samples. It can be observed that Y-doped samples show stronger light absorption properties in the UV region and the absorption edge shifts to a longer wavelength. The absorption in the visible region generally increases with the increase of Y-doped content. Modification of mesoporous titania with Y ion caused absorption spectra to shift to the visible region, it demonstrated that Y-doping was in favor of visible light absorption. For pure mesoporous titania, the absorption in the ultraviolet range ($\lambda = 378$ nm) was associated with the excitation of the O 2p electron to the Ti 3d level. The red shifts of the optical absorption edge to the visible light region can be attributed to the charge-transfer transition between the f electrons of Y ion and the titania valence or conduction band [21]. As a result, the Y-doped samples have trapping level which decreased the titania band gap, and the Y ions in the doped photocatalysts increased the visible light absorption ability of the photocatalysts. Moreover, because of rare earth elements possessing a broad absorption band, the effect of those incorporated into the titania was similar to adding a photosensitizer to the reaction solution. Therefore, the Y ions surrounding the titania grains could absorb a larger range of light radiation, which brings about the higher light absorption in the 420–700 nm region of the Y-doped samples [25].

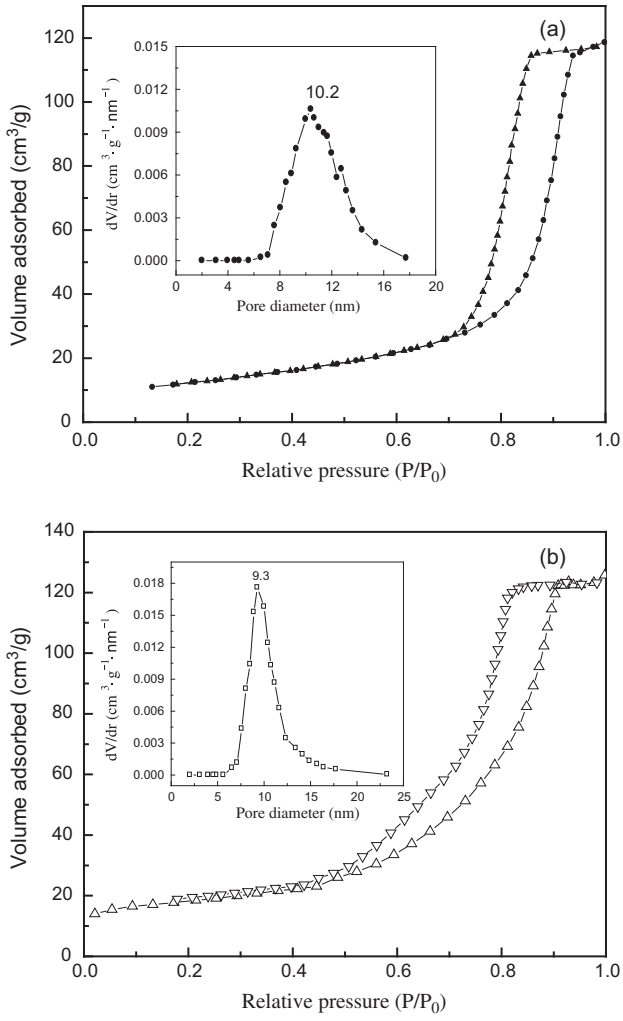

Fig. 3. N_2 adsorption–desorption isotherms and adsorption BJH pore size distribution plots for (a) $MTiO_2$ and (b) 0.20 mol% Y/$MTiO_2$/Fe_3O_4.

3.5. Effect of Y-doped content on the photocatalytic activity of Y/$MTiO_2$/Fe_3O_4

Fig. 5 shows the results of MB degradation with irradiation time under visible light irradiation in the presence of Y/$MTiO_2$/Fe_3O_4 with Y-doped content in the range of 0.10–0.40 mol%. It was showed that the photocatalytic activity of $MTiO_2$/Fe_3O_4 enhanced after Y-doping, the optimum content of Y-doping was 0.20 mol%. A possible mechanism for the photocatalytic enhancement is proposed as follows. The ionic radius of Y^{3+} is 0.088 nm, which is much larger than

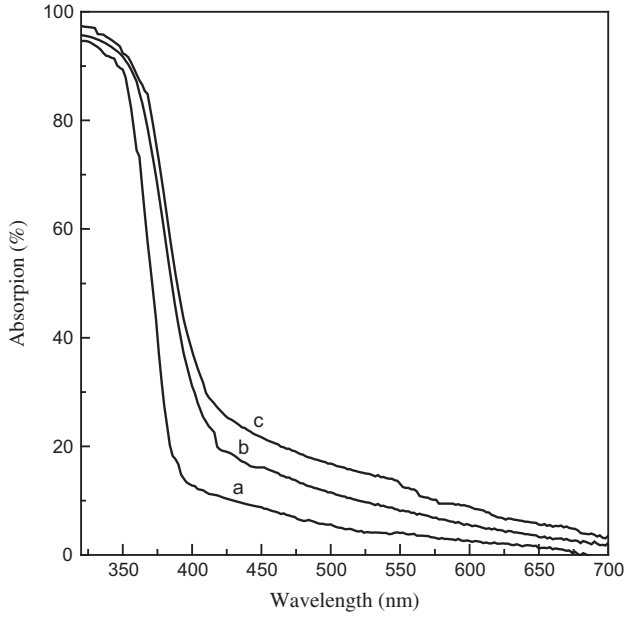

Fig. 4. UV–vis diffuse reflectance spectra of samples (a) $MTiO_2/Fe_3O_4$, (b) 0.10 mol% $Y/MTiO_2/Fe_3O_4$, and (c) 0.20 mol% $Y/MTiO_2/Fe_3O_4$.

that of Ti^{4+} (0.068 nm), thus it is hard for Y^{3+} to enter into the lattice of TiO_2. It was reported that rare earth salts were changed into rare earth oxides during the calcination process and these oxides could be uniformly adsorbed on the surface of TiO_2, which would be eventually beneficial to separate the charge carriers, prolong their lifetime and hinder the recombination of electron-hole pairs efficiently, and then improved its photocatalytic performance efficiently [21]. The increase of the photocatalytic activity with the increase of the content of Y-doping might be attributed to the electrons trapped in Y sites, which were subsequently transferred to the absorbed O_2. The photoactivity of the catalyst increased gradually with an enhancing in the content of Y-doping when the content of Y-doping was lower than 0.20 mol%. However, the photoactivity of the catalyst decreased when the content of Y-doping reached 0.30 mol%. This result could be attributed to the surrounding Y ions, which acted as recombination centers for the photogenerated electrons and holes at high doping. The more available Y ions with the higher Y-doping concentration will lead to lower photocatalytic activity.

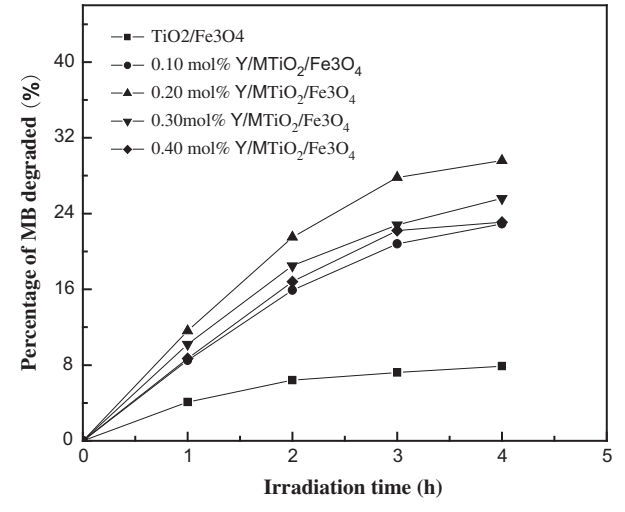

Fig. 5. Effect of Y-doped content on the degradation rate of MB.

The UV–vis absorption spectra showed that Y-doping improved the ultraviolet absorption and the red shift of the absorption profile, which was benefited to improve the photocatalytic activity of $MTiO_2/Fe_3O_4$. At the same time, rare earth elements have the ability of oxygen storage; they release oxygen to the reaction system when the concentration of oxygen in the system is low, whereas they can store oxygen [26]. It was known from the photocatalytic mechanism that oxygen adsorbed on photocatalyst could trap effectively the photogenerated electron [27], so the simple recombination between electron and hole was inhibited. The redox probability increased, and the photocatalytic activity enhanced.

3.6. Photocatalytic activity

Photocatalytic activity of Y-doped mesoprous titania samples was estimated by measuring the degradation rate of MB in the presence of visible light irradiation without concerning the degradation intermediates in detail. Pure mesoporous titania synthesized by the same method without any dopant was used as the reference system. It was found that MB concentration remained stable after 1 h of stirring without illumination in the presence of obtained samples.

In order to evaluate the actual photocatalytic activity of the $Y/MTiO_2/Fe_3O_4$ photocatalyst calcined at 500 °C for 2 h, comparison of two MB degradation processes, namely, photolysis and photocatalytic degradation by $Y/MTiO_2/Fe_3O_4$, by corresponding experiments to assess the effect of catalyst on the overall removal rate for an initial MB concentration of (50 mg/L), the results were shown in Fig. 6.

Experimental results showed that MB could be degraded at a certain degree under visible light irradiation (see Fig. 6(a)). The MB degradation rates increased with visible light irradiation for the $MB/Y/MTiO_2/Fe_3O_4$ system (Fig. 6(b)). By comparison of the amounts of MB removed with and without $Y/MTiO_2/Fe_3O_4$ (Fig. 6), it can be affirmed that the disappearance of MB

molecules was due to photocatalytic degradation by $Y/MTiO_2/Fe_3O_4$.

Fig. 7 shows the results of MB degradation with irradiation time under visible light irradiation in the presence of different photocatalysts. The results revealed two main observations: (1) the activity of the $MTiO_2/Fe_3O_4$ particle was lower than that of single phase $MTiO_2$ sample; (2) the Y-doping of $MTiO_2/Fe_3O_4$ resulted in higher photoactivity than pure $MTiO_2$ and $MTiO_2/Fe_3O_4$.

The lower photoactivity of $MTiO_2/Fe_3O_4$ compared to the pure $MTiO_2$ prepared by the same method could be ascribed to the electronic interactions between the two semiconductors, which has been described by others [28–30]. Electronic interactions occurred at the point of contact of the different phases (heterojunction), leading to the transfer of charge carriers across this junction when two or more semiconductors are in contact [27]. It is feasible for the photogenerated electrons in the excited TiO_2 to be transferred into the lower-lying conduction band of magnetite and the holes to be transferred to the upper-lying valence of this iron oxide. Taking into account the narrower band gap of magnetite (0.1 eV), this is believed to lead to an increase in the incidence of electron-hole recombination [31], so the photocatalytic activity of $MTiO_2/Fe_3O_4$ was reduced.

3.7. Cyclic performances of $Y/MTiO_2/Fe_3O_4$ for the degradation of MB

In order to test the cyclic usage possibility for the $Y/MTiO_2/Fe_3O_4$ photocatalyst, the photocatalytic degradation experiments of MB had been repeated for four cycles. The change in relative degradation percentage of MB with cycling operation was shown in Fig. 8. It was observed that the photocatalytic activity of the present photocatalyst was just slightly reduced in stirred aqueous solution, and the photocatalytic activity of $Y/MTiO_2/Fe_3O_4$ remained ca. 88% of its activity as-prepared after being used four times, the degradation percentage of MB could reach 25.64% when irradiation time was 4 h. Thus, it is suggested that the deposited $MTiO_2$ has firmly attached to the Fe_3O_4 surface, and could not be easily exfoliated from the Fe_3O_4 with mechanically stirred

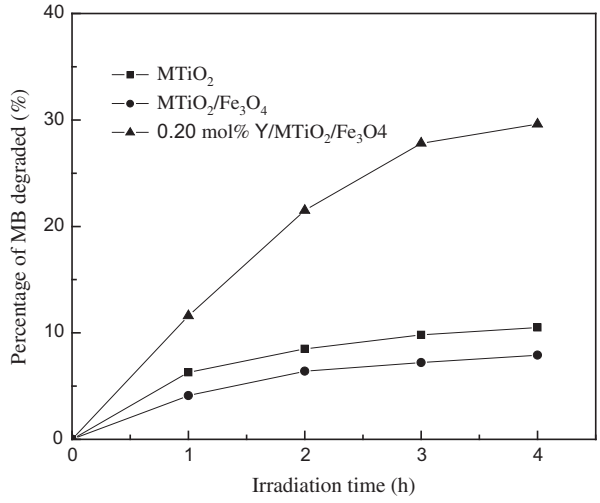

Fig. 7. Degradation curves of MB with visible light irradiation time.

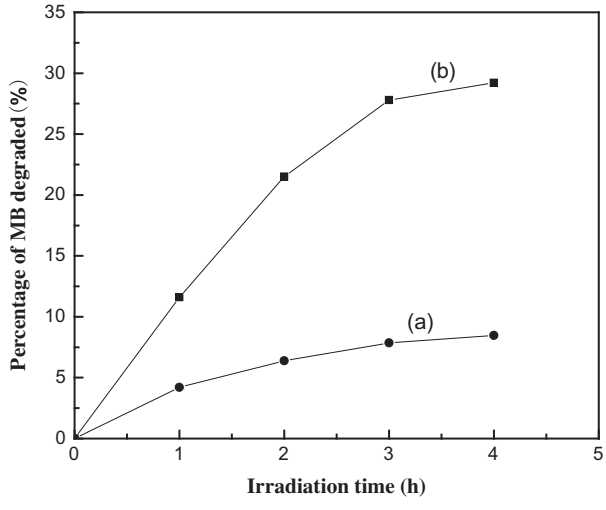

Fig. 6. Effect of photocatalyst on the removal rate of MB. (a) only with visible light irradiation and (b) 0.20 mol% $Y/MTiO_2/Fe_3O_4$ with visible light irradiation.

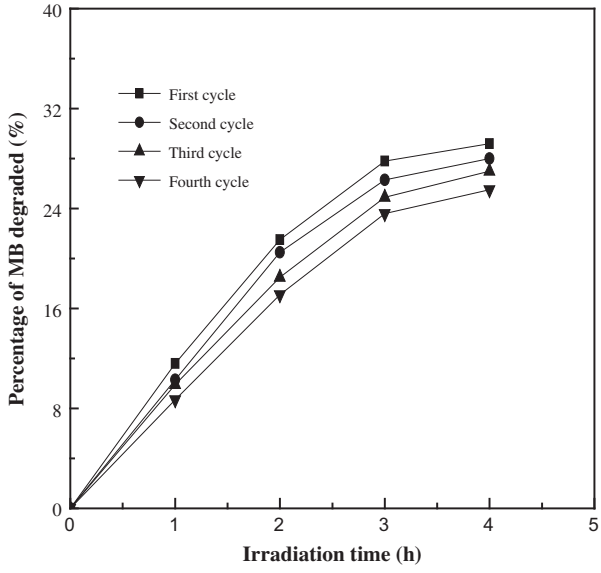

Fig. 8. The cyclic performance of 0.20 mol% $Y/MTiO_2/Fe_3O_4$.

solutions for a long period. At the same time, it also proved that the final removal of MB from solution was caused by the photocatalytic degradation other than the adsorption process that would lead to saturated adsorption of MB on the photocatalyst. These results indicated that cyclic usage of the $Y/MTiO_2/Fe_3O_4$ composite was possible and its stability in treating polluted water was satisfactory. Therefore, it is potentially employable for continuous photocatalytic degradation processes.

4. Conclusions

A composite photocatalyst ($Y/MTiO_2/Fe_3O_4$) was successfully prepared by coating photoactive $Y/MTiO_2$ onto a magnetic Fe_3O_4 core by template method using $Y(NO_3)_3{\cdot}6H_2O$ and $Ti(OBu)_4$ as precursors and Pluronic P123 as template in the presence of Fe_3O_4 particles. The photocatalyst thus prepared was applied to degrade model contaminated water of MB. The results showed that Y-doping enhanced the photocatalytic activity of $MTiO_2/Fe_3O_4$ under visible light irradiation, and 0.20 mol% Y-doped sample exhibited the optimum photocatalytic activity for MB degradation. The Y-doping caused absorption spectra of TiO_2/Fe_3O_4 to shift to the visible region. The photocatalyst could be separated easily by an external magnetic field and reused without any mass loss.

Acknowledgment

The authors gratefully acknowledge financial support for this work from the National Natural Science Foundation of China (41173119).

References

[1] I. Arslan, I.A. Balcioglu, D.W. Bahnemann, Heterogeneous photocatalytic treatment of simulated dyehouse effluents using novel TiO_2-photocatalyst, Appl. Catal. B 26 (2000) 193–206.
[2] S. Zheng, Q. Huang, J. Zhou, B. Wang, A study on dye photoremoval in TiO_2 suspension solution, J. Photochem. Photobiol., A 108 (1997) 235–243.
[3] A. Zaleska, J.W. Sobczak, E. Grabowska, J. Hupka, Preparation and photocatalytic activity of boron-modified TiO_2 under UV and visible light, Appl. Catal. B 78 (2008) 92–100.
[4] S. Adishkumar, S. Kanmani, Treatment of phenolic wastewaters in single baffle reactor by solar/TiO_2/H_2O_2 process, Desalin. Water Treat. 24 (2010) 67–73.
[5] I.J. Ochuma, R.P. Fishwick, J. Wood, J.M. Winterbottom, Photocatalytic oxidation of 2,4,6-trichlorophenol in water using a cocurrent downflow contactor reactor (CDCR), J. Hazard. Mater. 144 (2007) 627–633.
[6] A.C. Rodrigues, M. Boroski, N.S. Shimada, J.C. Garcia, J. Nozaki, N. Hioka, Treatment of paper pulp and paper mill wastewater by coagulation–flocculation followed by heterogeneous photocatalysis, J. Photochem. Photobiol., A 194 (2008) 1–10.
[7] T.L. Thompson, J.T. Yates, Surface science studies of the photoactivation of TiO_2. New photochemical processes, Chem. Rev. 106 (2006) 4428–4453.
[8] J. Yu, Y. Su, B. Cheng, M. Zhou, Effects of pH on the microstructures and photocatalytic activity of mesoporous nanocrystalline titania powders prepared via hydrothermal method, J. Mol. Catal. A: Chem. 258 (2006) 104–112.
[9] N. Koshitani, S. Sakulkhaemaruethai, Y. Suzuki, S. Yoshikawa, Preparation of mesoporous titania nanocrystals using alkylamine surfactant templates, Ceram. Int. 32 (2006) 819–824.
[10] A. Rachel, M. Subrahmanyam, P. Boule, Comparison of photocatalytic efficiencies of TiO_2 in suspended and immobilised form for the photocatalytic degradation of nitrobenzenesulfonic acids, Appl. Catal. B 37 (2002) 301–308.
[11] H. Hirashima, H. Imai, V. Balek, Preparation of mesoporous TiO_2 gels and their characterization, J. Non-Cryst. Solids 285 (2001) 96–100.
[12] P. Yang, D. Zhao, D.I. Margolese, B.F. Chmelka, G.D. Stucky, Block copolymer templating syntheses of mesoporous metal oxides with large ordering lengths and semicrystalline framework, Chem. Mater. 11 (1999) 2813–2826.
[13] J.C. Wu, C.H. Chen, A visible-light response vanadium-doped titania nanocatalyst by sol-gel method, J. Photochem. Photobiol., A 163 (2004) 509–515.
[14] C. Wang, C. Böttcher, D.W. Bahnemann, J.K. Dohrmann, In situ electron microscopy investigation of Fe(III)-doped TiO_2 nanoparticles in an aqueous environment, J. Nanopart. Res. 6 (2004) 119–122.
[15] B. Sun, E.P. Reddy, P.G. Smirniotis, Effect of the Cr^{6+} concentration in Cr-incorporated TiO_2-loaded MCM-41 catalysts for visible light photocatalysis, Appl. Catal. B 57 (2005) 139–149.
[16] W. Zhang, Y. Li, S. Zhu, F. Wang, Copper doping in titanium oxide catalyst film prepared by dereactive magnetron sputtering, Catal. Today 93–95 (2004) 589–594.
[17] J. Xu, M. Lu, X. Guo, H. Li, Zinc ions surface-doped titanium dioxide nanotubes and its photocatalysis activity for degradation of methyl orange in water, J. Mol. Catal. A: Chem. 226 (2005) 123–127.
[18] D.E. De Vos, M. Dams, B.F. Sels, P.A. Jacobs, Ordered mesoporous and microporous molecular sieves functionalized with transition metal complexes as catalysts for selective organic transformations, Chem. Rev. 102 (2002) 3615–3640.
[19] K.V. Baiju, C.P. Sibu, K. Rajesh, P. Krishna Pillai, P. Mukundan, K.G.K. Warrier, W. Wunderlich, An aqueous sol-gel route to synthesize nanosized lanthana-doped titania having an increased anatase phase stability for photocatalytic application, Mater. Chem. Phys. 90 (2005) 123–127.
[20] Y. Xie, C. Yuan, Visible-light responsive cerium ion modified titania sol and nanocrystallites for X-3B dye photodegradation, Appl. Catal. B 46 (2003) 251–259.
[21] A.W. Xu, Y. Gao, H.Q. Liu, The preparation, characterization, and their photocatalytic activities of rare-earth-doped TiO_2 nanoparticles, J. Catal. 207 (2002) 151–157.
[22] X.S. Niu, S.J. Li, H.H. Chu, J.G. Zhou, Preparation, characterization of Y- doped TiO_2 nanoparticles and their photocatalytic activities for methyl orange degradation, J. Rare Earths 29 (2011) 225–229.
[23] K.S.W. Sing, D.H. Everett, R.A.W. Haul, L. Moscou, R.A. Pierotti, J. Rouquerol, V.T. Siemieniewska, Reporting physisorption data for gas/solid systems with special reference to the determination of surface area and porosity, Pure Appl. Chem. 57 (1985) 603–619.
[24] F. Rojas, I. Kornhauser, C. Felipe, J.M. Esparza, S. Cordero, A. Dominguez, J.L. Riccardo, Capillary condensation in heterogeneous mesoporous networks consisting of variable connectivity and pore-size correlation, Phys. Chem. Chem. Phys. 4 (2002) 2346–2355.
[25] Y. Gao, A.W. Xu, J.Y. Zhu, Study on photocatalytic oxidation of nitrite over RE/TiO_2 photocatalysts, Chin. J. Catal. 22 (2001) 53–56.

[26] T. Yamada, K. Kayano, M. Funabiki, Platinum metals-ceria synergism in autoexhaust catalyst, Stud. Surf. Sci. Catal. 77 (1993) 329–332.
[27] H. Gerischer, A. Heller, The role of oxygen in photooxidation of organic molecules on semiconductor particles, J. Phys. Chem. 95 (1991) 5261–5267.
[28] D. Beydoun, R. Amal, G. Low, S. McEvoy, Occurrence and prevention of photodissolution at the phase junction of magnetite and titanium dioxide, J. Mol. Catal. A: Chem. 180 (2002) 193–200.
[29] J. Navio, M. Macias, M. Gonzalez-Catalan, A. Justo, Bulk and surface characterization of powder iron-doped titania photocatalysts, J. Mater. Sci. 27 (1992) 3036–30422.
[30] K.T. Ranjit, B. Viswanthan, Synthesis, characterization and photocatalytic properties of iron-doped TiO_2 catalysts, J. Photochem. Photobiol., A 108 (1997) 79–84.
[31] D. Beydoun, R. Amal, Novel photocatalyst: Titania-coated magnetite activity and photodissolution, J. Phys. Chem. B 104 (2000) 4387–4396.